System-size dependence of open-heavy-flavor production in nucleus-nucleus collisions at $\sqrt{s_{NN}} = 200$ GeV

A. Adare,[11] S. Afanasiev,[27] C. Aidala,[12,38] N. N. Ajitanand,[55] Y. Akiba,[49,50] H. Al-Bataineh,[43] J. Alexander,[55] K. Aoki,[31,49] N. Apadula,[25,56] L. Aphecetche,[57] R. Armendariz,[43] S. H. Aronson,[6] J. Asai,[50] E. T. Atomssa,[32] R. Averbeck,[56] T. C. Awes,[45] B. Azmoun,[6] V. Babintsev,[21] G. Baksay,[17] L. Baksay,[17] A. Baldisseri,[14] K. N. Barish,[7] P. D. Barnes,[35,*] B. Bassalleck,[42] S. Bathe,[4,7] S. Batsouli,[45] V. Baublis,[48] S. Baumgart,[49] A. Bazilevsky,[6] S. Belikov,[6,*] R. Bennett,[56] Y. Berdnikov,[52] A. A. Bickley,[11] J. G. Boissevain,[35] H. Borel,[14] K. Boyle,[56] M. L. Brooks,[35] H. Buesching,[6] V. Bumazhnov,[21] G. Bunce,[6,50] S. Butsyk,[35,56] S. Campbell,[56] B. S. Chang,[65] J.-L. Charvet,[14] S. Chernichenko,[21] C. Y. Chi,[12] J. Chiba,[28] M. Chiu,[22] I. J. Choi,[65] T. Chujo,[61] P. Chung,[55] A. Churyn,[21] V. Cianciolo,[45] C. R. Cleven,[19] B. A. Cole,[12] M. P. Comets,[46] P. Constantin,[35] M. Csanád,[16] T. Csörgő,[64] T. Dahms,[56] K. Das,[18] G. David,[6] M. B. Deaton,[1] K. Dehmelt,[17] H. Delagrange,[57,*] A. Denisov,[21] D. d'Enterria,[12] A. Deshpande,[50,56] E. J. Desmond,[6] O. Dietzsch,[53] A. Dion,[56] M. Donadelli,[53] O. Drapier,[32] A. Drees,[56] A. K. Dubey,[63] J. M. Durham,[35] A. Durum,[21] V. Dzhordzhadze,[7] Y. V. Efremenko,[45] J. Egdemir,[56] F. Ellinghaus,[11] W. S. Emam,[7] A. Enokizono,[34] H. En'yo,[49,50] S. Esumi,[60] K. O. Eyser,[7] D. E. Fields,[42,50] M. Finger,[8,27] M. Finger, Jr.,[8,27] F. Fleuret,[32] S. L. Fokin,[30] Z. Fraenkel,[63,*] J. E. Frantz,[44,56] A. Franz,[6] A. D. Frawley,[18] K. Fujiwara,[49] Y. Fukao,[31,49] T. Fusayasu,[41] S. Gadrat,[36] I. Garishvili,[58] A. Glenn,[11] H. Gong,[56] M. Gonin,[32] J. Gosset,[14] Y. Goto,[49,50] R. Granier de Cassagnac,[32] N. Grau,[2,25] S. V. Greene,[61] M. Grosse Perdekamp,[22,50] T. Gunji,[10] H.-Å. Gustafsson,[37,*] T. Hachiya,[20] A. Hadj Henni,[57] C. Haegemann,[42] J. S. Haggerty,[6] H. Hamagaki,[10] R. Han,[47] H. Harada,[20] E. P. Hartouni,[34] K. Haruna,[20] E. Haslum,[37] R. Hayano,[10] X. He,[19] M. Heffner,[34] T. K. Hemmick,[56] T. Hester,[7] H. Hiejima,[22] J. C. Hill,[25] R. Hobbs,[42] M. Hohlmann,[17] W. Holzmann,[55] K. Homma,[20] B. Hong,[29] T. Horaguchi,[49,59] D. Hornback,[58] T. Ichihara,[49,50] H. Iinuma,[31,49] K. Imai,[26,31,49] M. Inaba,[60] Y. Inoue,[49,51] D. Isenhower,[1] L. Isenhower,[1] M. Ishihara,[49] T. Isobe,[10] M. Issah,[55] A. Isupov,[27] B. V. Jacak,[56] J. Jia,[12] J. Jin,[12] O. Jinnouchi,[50] B. M. Johnson,[6] K. S. Joo,[40] D. Jouan,[46] F. Kajihara,[10] S. Kametani,[10,62] N. Kamihara,[49] J. Kamin,[56] M. Kaneta,[50] J. H. Kang,[65] H. Kanou,[49,59] D. Kawall,[50] A. V. Kazantsev,[30] A. Khanzadeev,[48] J. Kikuchi,[62] D. H. Kim,[40] D. J. Kim,[65] E. Kim,[54] E. Kinney,[11] Á. Kiss,[16] E. Kistenev,[6] A. Kiyomichi,[49] J. Klay,[34] C. Klein-Boesing,[39] L. Kochenda,[48] V. Kochetkov,[21] B. Komkov,[48] M. Konno,[60] D. Kotchetkov,[7] A. Kozlov,[63] A. Král,[13] A. Kravitz,[12] J. Kubart,[8,24] G. J. Kunde,[35] N. Kurihara,[10] K. Kurita,[49,51] M. J. Kweon,[29] Y. Kwon,[65,58] G. S. Kyle,[43] R. Lacey,[55] Y. S. Lai,[12] J. G. Lajoie,[25] A. Lebedev,[25] D. M. Lee,[35] M. K. Lee,[65] T. Lee,[54] M. J. Leitch,[35] M. A. L. Leite,[53] B. Lenzi,[53] X. Li,[9] T. Liška,[13] A. Litvinenko,[27] M. X. Liu,[35] B. Love,[61] D. Lynch,[6] C. F. Maguire,[61] Y. I. Makdisi,[5] A. Malakhov,[27] M. D. Malik,[42] V. I. Manko,[30] Y. Mao,[47,49] L. Mašek,[8,24] H. Masui,[60] F. Matathias,[12] M. McCumber,[56] P. L. McGaughey,[35] D. McGlinchey,[11] Y. Miake,[60] P. Mikeš,[8,24] K. Miki,[60] T. E. Miller,[61] A. Milov,[56] S. Mioduszewski,[6] M. Mishra,[3] J. T. Mitchell,[6] M. Mitrovski,[55] A. Morreale,[7] D. P. Morrison,[6,†] T. V. Moukhanova,[30] D. Mukhopadhyay,[61] J. Murata,[49,51] S. Nagamiya,[28] Y. Nagata,[60] J. L. Nagle,[11,‡] M. Naglis,[63] I. Nakagawa,[49,50] Y. Nakamiya,[20] T. Nakamura,[20] K. Nakano,[49,59] J. Newby,[34] M. Nguyen,[56] B. E. Norman,[35] R. Nouicer,[6] A. S. Nyanin,[30] E. O'Brien,[6] S. X. Oda,[10] C. A. Ogilvie,[25] H. Ohnishi,[49] M. Oka,[60] K. Okada,[50] O. O. Omiwade,[1] A. Oskarsson,[37] M. Ouchida,[20] K. Ozawa,[10] R. Pak,[6] D. Pal,[61] A. P. T. Palounek,[35] V. Pantuev,[23,56] V. Papavassiliou,[43] J. Park,[54] W. J. Park,[29] S. F. Pate,[43] H. Pei,[25] J.-C. Peng,[22] H. Pereira,[14] V. Peresedov,[27] D.Yu. Peressounko,[30] C. Pinkenburg,[6] M. L. Purschke,[6] A. K. Purwar,[35] H. Qu,[19] J. Rak,[42] A. Rakotozafindrabe,[32] I. Ravinovich,[63] K. F. Read,[45,58] S. Rembeczki,[17] M. Reuter,[56] K. Reygers,[39] V. Riabov,[48] Y. Riabov,[48] G. Roche,[36] A. Romana,[32,*] M. Rosati,[25] S. S. E. Rosendahl,[37] P. Rosnet,[36] P. Rukoyatkin,[27] V. L. Rykov,[49] B. Sahlmueller,[39,56] N. Saito,[31,49,50] T. Sakaguchi,[6] S. Sakai,[60] H. Sakata,[20] V. Samsonov,[48] S. Sato,[26,28] S. Sawada,[28] J. Seele,[11] R. Seidl,[22] V. Semenov,[21] R. Seto,[7] D. Sharma,[63] I. Shein,[21] A. Shevel,[48,55] T.-A. Shibata,[49,59] K. Shigaki,[20] M. Shimomura,[60] K. Shoji,[31,49] A. Sickles,[56] C. L. Silva,[53] D. Silvermyr,[45] C. Silvestre,[14] K. S. Sim,[29] C. P. Singh,[3] V. Singh,[3] S. Skutnik,[25] M. Slunečka,[8,27] A. Soldatov,[21] R. A. Soltz,[34] W. E. Sondheim,[35] S. P. Sorensen,[58] I. V. Sourikova,[6] F. Staley,[14] P. W. Stankus,[45] E. Stenlund,[37] M. Stepanov,[43] A. Ster,[64] S. P. Stoll,[6] T. Sugitate,[20] C. Suire,[46] J. Sziklai,[64] T. Tabaru,[50] S. Takagi,[60] E. M. Takagui,[53] A. Taketani,[49,50] Y. Tanaka,[41] K. Tanida,[49,50,54] M. J. Tannenbaum,[6] A. Taranenko,[55] P. Tarján,[15] T. L. Thomas,[42] M. Togawa,[31,49] A. Toia,[56] J. Tojo,[49] L. Tomášek,[24] H. Torii,[49] R. S. Towell,[1] V-N. Tram,[32] I. Tserruya,[63] Y. Tsuchimoto,[20] C. Vale,[25] H. Valle,[61] H. W. van Hecke,[35] J. Velkovska,[61] R. Vértesi,[15] A. A. Vinogradov,[30] M. Virius,[13] V. Vrba,[24] E. Vznuzdaev,[48] M. Wagner,[31,49] D. Walker,[56] X. R. Wang,[43] Y. Watanabe,[49,50] J. Wessels,[39] S. N. White,[6] D. Winter,[12] C. L. Woody,[6] M. Wysocki,[11] W. Xie,[50] Y. L. Yamaguchi,[62] A. Yanovich,[21] Z. Yasin,[7] J. Ying,[19] S. Yokkaichi,[49,50] G. R. Young,[45] I. Younus,[33,42] I. E. Yushmanov,[30] W. A. Zajc,[12] O. Zaudtke,[39] C. Zhang,[45] S. Zhou,[9] J. Zimányi,[64,*] and L. Zolin[27]

(PHENIX Collaboration)

[1]*Abilene Christian University, Abilene, Texas 79699, USA*

[2]*Department of Physics, Augustana College, Sioux Falls, South Dakota 57197, USA*

[3]*Department of Physics, Banaras Hindu University, Varanasi 221005, India*

[4]*Baruch College, City University of New York, New York, New York 10010, USA*

[5]*Collider-Accelerator Department, Brookhaven National Laboratory, Upton, New York 11973-5000, USA*

[6]*Brookhaven National Laboratory, Upton, New York 11973-5000, USA*

[7]*University of California-Riverside, Riverside, California 92521, USA*
[8]*Charles University, Ovocný trh 5, Praha 1, 116 36 Prague, Czech Republic*
[9]*Science and Technology on Nuclear Data Laboratory, China Institute of Atomic Energy, Beijing 102413, People's Republic of China*
[10]*Center for Nuclear Study, Graduate School of Science, University of Tokyo, 7-3-1 Hongo, Bunkyo, Tokyo 113-0033, Japan*
[11]*University of Colorado, Boulder, Colorado 80309, USA*
[12]*Columbia University, New York, New York 10027 and Nevis Laboratories, Irvington, New York 10533, USA*
[13]*Czech Technical University, Zikova 4, 166 36 Prague 6, Czech Republic*
[14]*Dapnia, CEA Saclay, F-91191 Gif-sur-Yvette, France*
[15]*Debrecen University, H-4010 Debrecen, Egyetem tér 1, Hungary*
[16]*ELTE, Eötvös Loránd University, H-1117 Budapest, Pázmány Péter sétány 1/A, Hungary*
[17]*Florida Institute of Technology, Melbourne, Florida 32901, USA*
[18]*Florida State University, Tallahassee, Florida 32306, USA*
[19]*Georgia State University, Atlanta, Georgia 30303, USA*
[20]*Hiroshima University, Kagamiyama, Higashi-Hiroshima 739-8526, Japan*
[21]*IHEP Protvino, State Research Center of Russian Federation, Institute for High Energy Physics, Protvino 142281, Russia*
[22]*University of Illinois at Urbana-Champaign, Urbana, Illinois 61801, USA*
[23]*Institute for Nuclear Research of the Russian Academy of Sciences, prospekt 60-letiya Oktyabrya 7a, Moscow 117312, Russia*
[24]*Institute of Physics, Academy of Sciences of the Czech Republic, Na Slovance 2, 182 21 Prague 8, Czech Republic*
[25]*Iowa State University, Ames, Iowa 50011, USA*
[26]*Advanced Science Research Center, Japan Atomic Energy Agency, 2-4 Shirakata Shirane, Tokai-mura, Naka-gun, Ibaraki-ken 319-1195, Japan*
[27]*Joint Institute for Nuclear Research, 141980 Dubna, Moscow Region, Russia*
[28]*KEK, High Energy Accelerator Research Organization, Tsukuba, Ibaraki 305-0801, Japan*
[29]*Korea University, Seoul 136-701, Korea*
[30]*Russian Research Center "Kurchatov Institute," Moscow 123098, Russia*
[31]*Kyoto University, Kyoto 606-8502, Japan*
[32]*Laboratoire Leprince-Ringuet, Ecole Polytechnique, CNRS-IN2P3, Route de Saclay, F-91128 Palaiseau, France*
[33]*Physics Department, Lahore University of Management Sciences, Lahore 54792, Pakistan*
[34]*Lawrence Livermore National Laboratory, Livermore, California 94550, USA*
[35]*Los Alamos National Laboratory, Los Alamos, New Mexico 87545, USA*
[36]*LPC, Université Blaise Pascal, CNRS-IN2P3, Clermont-Fd, 63177 Aubiere Cedex, France*
[37]*Department of Physics, Lund University, Box 118, SE-221 00 Lund, Sweden*
[38]*Department of Physics, University of Michigan, Ann Arbor, Michigan 48109-1040, USA*
[39]*Institut für Kernphysik, University of Muenster, D-48149 Muenster, Germany*
[40]*Myongji University, Yongin, Kyonggido 449-728, Korea*
[41]*Nagasaki Institute of Applied Science, Nagasaki-shi, Nagasaki 851-0193, Japan*
[42]*University of New Mexico, Albuquerque, New Mexico 87131, USA*
[43]*New Mexico State University, Las Cruces, New Mexico 88003, USA*
[44]*Department of Physics and Astronomy, Ohio University, Athens, Ohio 45701, USA*
[45]*Oak Ridge National Laboratory, Oak Ridge, Tennessee 37831, USA*
[46]*IPN-Orsay, Universite Paris Sud, CNRS-IN2P3, BP1, F-91406 Orsay, France*
[47]*Peking University, Beijing 100871, People's Republic of China*
[48]*PNPI, Petersburg Nuclear Physics Institute, Gatchina, Leningrad Region 188300, Russia*
[49]*RIKEN Nishina Center for Accelerator-Based Science, Wako, Saitama 351-0198, Japan*
[50]*RIKEN BNL Research Center, Brookhaven National Laboratory, Upton, New York 11973-5000, USA*
[51]*Physics Department, Rikkyo University, 3-34-1 Nishi-Ikebukuro, Toshima, Tokyo 171-8501, Japan*
[52]*Saint Petersburg State Polytechnic University, St. Petersburg 195251, Russia*
[53]*Universidade de São Paulo, Instituto de Física, Caixa Postal 66318, São Paulo CEP05315-970, Brazil*
[54]*Seoul National University, Seoul, Korea*
[55]*Chemistry Department, Stony Brook University, SUNY, Stony Brook, New York 11794-3400, USA*
[56]*Department of Physics and Astronomy, Stony Brook University, SUNY, Stony Brook, New York 11794-3400, USA*
[57]*SUBATECH (Ecole des Mines de Nantes, CNRS-IN2P3, Université de Nantes) BP 20722-44307, Nantes, France*
[58]*University of Tennessee, Knoxville, Tennessee 37996, USA*
[59]*Department of Physics, Tokyo Institute of Technology, Oh-okayama, Meguro, Tokyo 152-8551, Japan*
[60]*Institute of Physics, University of Tsukuba, Tsukuba, Ibaraki 305, Japan*
[61]*Vanderbilt University, Nashville, Tennessee 37235, USA*
[62]*Waseda University, Advanced Research Institute for Science and Engineering, 17 Kikui-cho, Shinjuku-ku, Tokyo 162-0044, Japan*
[63]*Weizmann Institute, Rehovot 76100, Israel*

[64] *Institute for Particle and Nuclear Physics, Wigner Research Centre for Physics, Hungarian Academy of Sciences (Wigner RCP, RMKI) H-1525 Budapest 114, PO Box 49, Budapest, Hungary*
[65] *Yonsei University, IPAP, Seoul 120-749, Korea*
(Received 31 October 2013; revised manuscript received 19 July 2014; published 5 September 2014)

The PHENIX Collaboration at the Relativistic Heavy Ion Collider has measured open-heavy-flavor production in Cu + Cu collisions at $\sqrt{s_{NN}} = 200$ GeV through the measurement of electrons at midrapidity that originate from semileptonic decays of charm and bottom hadrons. In peripheral Cu + Cu collisions an enhanced production of electrons is observed relative to $p + p$ collisions scaled by the number of binary collisions. In the transverse momentum range from 1 to 5 GeV/c the nuclear modification factor is $R_{AA} \sim 1.4$. As the system size increases to more central Cu + Cu collisions, the enhancement gradually disappears and turns into a suppression. For $p_T > 3$ GeV/c, the suppression reaches $R_{AA} \sim 0.8$ in the most central collisions. The p_T and centrality dependence of R_{AA} in Cu + Cu collisions agree quantitatively with R_{AA} in d + Au and Au + Au collisions, if compared at a similar number of participating nucleons $\langle N_{\rm part} \rangle$.

DOI: 10.1103/PhysRevC.90.034903 PACS number(s): 25.75.Cj

I. INTRODUCTION

Studies of the hot matter formed in ultrarelativistic heavy-ion collisions, such as those produced at the Relativistic Heavy Ion Collider (RHIC), require experimental probes, like heavy quarks (charm and bottom), that are produced during the collisions. The temperature of the matter produced in $A + A$ collisions [1,2] is much less than that of the heavy quark masses ($m_c \sim 1.3$ GeV, $m_b \sim 4.2$ GeV). Thus, charm and bottom quarks will only be produced in the initial stage of the collision, rather than through thermal excitation or other mechanisms. Once produced, they propagate through the hot matter and their kinematic distributions are modified through interactions along their path. These medium transport effects can be studied experimentally through the spectra of decay products from hadrons with heavy quark content.

Indeed, a large suppression of high transverse momentum (p_T) electrons from semileptonic heavy-flavor decays was discovered in Au + Au collisions at $\sqrt{s_{NN}} = 200$ GeV relative to $p + p$ collisions [3–5], contrary to original predictions [6]. It is most pronounced in central collisions, i.e., collisions with small impact parameters, and disappears in more peripheral events. The suppression of heavy flavor at high p_T was widely interpreted as evidence that heavy-flavor quarks lose a significant amount of energy as they traverse hot matter [7–9]. Additional suppression effects have been taken into account in different theoretical calculations [10–15] with varied success. These models can be additionally constrained by comparing to heavy-flavor electron spectra at different rapidities or system sizes.

Comparing to $p + p$ collisions alone is not sufficient to extract hot-nuclear-matter effects. The presence of the nuclear environment can alter the kinematic distributions without hot matter ever being formed. Such alterations in the absence of hot matter, whether they trace back to the incoming nuclei or to interactions with the nuclear environment after heavy quarks are formed, are generally referred to as "cold-nuclear-matter effects." For example, modifications of the parton distributions in bound nucleons will affect the production rates of particles [16]. Initial-state parton scattering and energy loss in the nucleus will also affect the observed particle spectra [17].

Evidence for such nuclear effects was shown by PHENIX in data from d + Au collisions at $\sqrt{s_{NN}} = 200$ GeV, where an enhancement of electrons from heavy-flavor decays was observed relative to $p + p$ collisions [18] between $1 < p_T < 5$ GeV/c. The enhancement depends on centrality; as the collisions become more central, the enhancement becomes more and more pronounced, in contrast to the increasing suppression observed in Au + Au collisions at the same $\sqrt{s_{NN}}$.

Until recently, the study of $p + A$ and $d + A$ collisions was considered the best way to investigate and quantify these cold-nuclear-matter effects. This assumption is now challenged by recent results obtained in p + Pb and d + Au collisions pointing to additional phenomena that may come from hydrodynamics [19–22] or gluon saturation [23–26], among others. Therefore, careful comparison of results from $p + p$, $p + A$, $d + A$, and $A + A$ collisions is likely needed to isolate an unambiguous signature of hot nuclear matter.

At RHIC, effects from cold and hot nuclear matter compete and their relative importance likely depends on the system size, which can be quantified through the average number of binary nucleon-nucleon collisions ($\langle N_{\rm coll} \rangle$) or the average number of participants ($\langle N_{\rm part} \rangle$). Using $\langle N_{\rm coll} \rangle$, central d + Au collisions show the largest enhancement at $N_{\rm coll} \sim 15$, while central Au + Au collisions exhibit the largest suppression at $N_{\rm coll} \sim 1000$ (see Table I). To further investigate system-size dependence, PHENIX has studied Cu + Cu collisions, also at $\sqrt{s_{NN}} = 200$ GeV. The $\langle N_{\rm coll} \rangle$ range for this intermediate-sized system overlaps with d + Au as well as Au + Au collisions and thus Cu + Cu allows access to the transition region between the dominance of enhancement effects and hot-nuclear-matter suppression.

In this paper we present data of single electrons (we refer to electrons to mean the sum of electrons and positrons divided by two) from semileptonic decays of heavy-flavor hadrons obtained in Cu + Cu collisions at $\sqrt{s_{NN}} = 200$ GeV. The paper is organized as follows. Section II presents the

*Deceased.
†PHENIX Co-Spokesperson: morrison@bnl.gov
‡PHENIX Co-Spokesperson: jamie.nagle@colorado.edu

TABLE I. The average number of binary collisions ($\langle N_{\rm coll}\rangle$) and participating nucleons ($\langle N_{\rm part}\rangle$) for $d+$Au, Cu + Cu, and Au + Au collisions at $\sqrt{s_{NN}} = 200$ GeV. $\langle N_{\rm part}\rangle$ and $\langle N_{\rm coll}\rangle$ increase with decreasing impact parameter (more central events).

Colliding species	Centrality (%)	$\langle N_{\rm coll}\rangle$	$\langle N_{\rm part}\rangle$
$d+$Au	0–100	7.59 ± 0.43	9.1 ± 0.4
	0–20	15.06 ± 1.01	15.4 ± 1.0
	20–40	10.25 ± 0.70	10.6 ± 0.7
	40–60	6.58 ± 0.44	7.0 ± 0.6
	60–88	3.20 ± 0.19	3.1 ± 0.3
Cu + Cu	0–94	51.8 ± 5.6	34.6 ± 1.2
	0–10	182.7 ± 20.7	98.2 ± 2.4
	0–20	151.8 ± 17.1	85.9 ± 2.3
	20–40	61.2 ± 6.6	45.2 ± 1.7
	40–60	22.3 ± 2.9	21.2 ± 1.4
	60–94	5.1 ± 0.7	6.4 ± 0.4
Au + Au	0–92	257.8 ± 25.4	109.1 ± 4.1
	0–10	955.4 ± 93.6	352.2 ± 3.3
	10–20	602.6 ± 59.3	234.6 ± 4.7
	20–40	296.8 ± 31.1	140.4 ± 4.9
	40–60	90.70 ± 11.8	59.95 ± 3.6
	60–92	14.50 ± 4.00	14.5 ± 2.5

experimental setup and describes how we measure the inclusive yield of electrons and positrons. In Sec. III we discuss how we extract the heavy-flavor contribution from the inclusive yield. The results are presented in Sec. IV and discussed and compared to previous results in Sec. V and theoretical models in Sec. VI. Section VII gives a summary of this work.

II. EXPERIMENTAL METHODS

Figure 1 shows the layout of the 2005 PHENIX detector. Electrons and positrons are measured using the two central spectrometer arms, each of which covers the pseudorapidity range of $|\eta| < 0.35$ with an azimuthal coverage of $\Delta\phi = \pi/2$. Charged tracks are reconstructed radially outside of an axial magnetic field using layers of drift chambers and pad

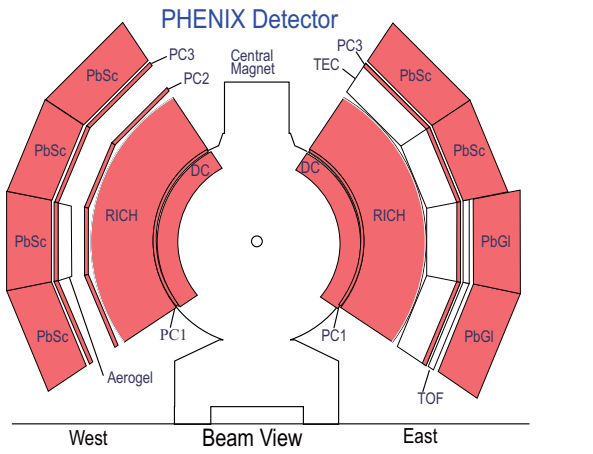

FIG. 1. (Color online) Beam view of the PHENIX central arm detector in the 2005 configuration.

chambers. Electrons are identified by hits in the ring imaging Čerenkov counter (RICH) and by requiring a match between an energy deposit in the electromagnetic calorimeter (EMCal) and the track's momentum. The RICH uses CO_2 gas at atmospheric pressure as the Čerenkov radiator. Electrons and pions begin to radiate in the RICH at $p_T > 20$ MeV/c and $p_T > 4.9$ GeV/c, respectively. The EMCal comprises four sectors in each arm. The two lowest sectors of the east arm are lead-glass and the remaining six are lead-scintillator. The angular segmentation of the lead-scintillator (lead-glass) is $\Delta\phi x \Delta\eta \sim 0.01 \times 0.01$ [0.008×0.008] and the energy resolution is $\delta E/E \sim 4.5\% \oplus 8.3/\sqrt{E(\text{GeV})}\%$ [$4.3\% \oplus 7.7/\sqrt{E(\text{GeV})}\%$]. A bag filled with He gas at atmospheric pressure is placed between the beam pipe and the drift chamber (DC) entrance window to minimize photon conversions. Detailed descriptions of the PHENIX detector subsystems can be found in Ref. [27].

For this analysis two different event samples were used. The first sample was obtained with a minimum-bias (MB) trigger, which registers all Cu + Cu collisions with a coincidence of at least one particle detected in each of the two beam-beam counters (BBCs). The BBCs are located at ± 1.44 m ($3.0 < |\eta| < 3.9$) and comprise 64 Čerenkov counter modules. Only events with a vertex position within ± 20 cm of the nominal $z = 0$ collision point are kept, giving a sample of 5.08×10^8 events. A second sample was collected with an additional trigger condition requiring the detection of an electron candidate in the event. This electron trigger (ERT) requires a coincidence between the EMCal and RICH detectors and provides an additional 3.3×10^9 events. For the ERT trigger, a threshold on the EMCal energy was set at approximately 1.2 GeV. In our analysis we only use electron candidates from this sample above $p_T > 3$ GeV/c, well beyond the point where the trigger reaches its maximum efficiency. The ERT trigger efficiency for electrons over all EMCal sectors was determined to be $67\% \pm 3\%$. The largest source of inefficiency comes from dead trigger tiles.

Centrality is determined by Monte Carlo calculation of the Glauber Model [28,29] using the measured charge deposited in the BBC. The MB collisions correspond to 0%–94% of the inelastic cross section. It is divided into centrality classes covering 0%–10%, 0%–20%, 20%–40%, 40%–60%, and 60%–94% of the centrality range (see Table I).

The analysis method used here, with some differences, is described in detail in Ref. [3]. Electron candidates start with charged tracks reconstructed by the DCs and pad chambers. These tracks are then identified as electrons by passing a set of electron identification (eID) cuts. First the track is projected to the RICH and at least five photomultiplier tubes containing one registered signal are required in a disk ($r = 11$ cm), with an angular size of 0.044 rad, centered at the projection point. This analysis uses a disk to reduce sensitivity to any possible mirror misalignment. The use of a tight RICH cut ensures a negligible contamination of hadrons with p_T above the RICH radiator threshold ($p_T > 4.9$ GeV/c for pions) through the p_T range (<7 GeV/c) of this analysis. The track is then projected to the EMCal and a 3σ cut is made on the difference between the projection and the center of the energy deposition.

A cut is also made on the shape of the EMCal shower, called prob, calculated from the deviation between the actual tower energy distribution and the expected distribution for an electromagnetic shower and normalized to be between 0 and 1. We require prob > 0.01 which has a 99% efficiency for an electromagnetic shower while rejecting a large fraction of hadrons. Finally, a cut is made on the ratio of the energy deposited in the EMCal to the momentum determined by the DC, represented by E/p. An electron deposits most of its energy in the EMCal and because its mass is so small, $E \approx p$ and E/p for an electron will be close to 1. The E/p cut is made symmetrically around 1 (between 0.8 and 1.2).

Though the eID cuts give a good sample of electrons, in a high-multiplicity environment overlap in the detectors can cause hadrons to be misidentified as electrons. The number and properties of those fake tracks reconstructed by random association can be obtained by exchanging, in software, the North and South halves of the RICH. For example, DC tracks from the South are matched with the RICH North and vice versa. After the swap, there cannot be any actual tracks, and all reconstructed ones are, by definition, fake tracks. The active area of the North and South RICH detectors are identical within ≈1%. In peripheral collisions, 3% of all tracks are mismatches, and in the central collisions that fraction rises to 22%.

A GEANT simulation of the full PHENIX detector was used to determine the extrapolation to full azimuthal acceptance and the correction for electron detection efficiency. The same eID and fiducial cuts are made on the simulation output and the data. The simulated electrons were generated flat in p_T to give sufficient statistics at high momentum and then weighted with a realistic p_T distribution to account for momentum smearing effects owing to the finite momentum resolution of the drift chamber.

III. ISOLATING THE HEAVY-FLAVOR YIELD

The inclusive single-electron spectrum has contributions from a multitude of sources, of which heavy-flavor decays constitute only one. Below 2 GeV/c, more than 50% of electrons come from decays of light mesons (dominated by the neutral pion Dalitz decay, $\pi^0 \to \gamma e^+ e^-$) [30]. Electrons from conversions of decay photons are also significant. However, the low-material design of the PHENIX detector minimizes this contribution to less than half of that from Dalitz decays (∼20% over the measured p_T range). Direct photons can also be a significant contribution to the inclusive electron spectrum (up to 20% at the highest p_T), either through conversions of real photons in material or manifestations of virtual photons as an e^+e^- pair. This group of electrons is collectively known as "photonic" electrons, owing to their origins with either a real or virtual direct or decay photon.

The other class of electrons, known as "nonphotonic," is dominated by the decays of open-heavy-flavor hadrons. The dielectron decays of the ρ, ω, and ϕ mesons contribute to the inclusive electron sample at the few percent level. Decays of quarkonia, dominated by $J/\psi \to e^+e^-$ [31], account for 20% of the electron yield above 4 GeV/c. Misreconstructed electron tracks from kaon decays ($K \to e\pi\nu$, referred to as K_{e3}) away from the collision vertex are ∼10% of the inclusive electrons at $p_T < 1$ GeV/c, but are negligible at higher p_T. Electron pairs produced via the Drell-Yan process contribute a negligibly small background to the heavy-flavor signal. To isolate the contribution of open-heavy-flavor decays to the inclusive electron spectrum, these backgrounds must be determined and removed from the inclusive electron sample. The methods for isolating the open-heavy-flavor electron yield used in this measurement are described in detail in Ref. [3] and are summarized here for completeness.

The first method calculates a cocktail of electrons from the nonheavy-flavor sources. Because the PHENIX experiment is a multipurpose detector, most of the dominant sources of single electrons have previously been measured in the same experiment. The largest background source comes from the neutral pion, both the Dalitz decay and the conversion of photons from the $\pi^0 \to \gamma\gamma$ decay. Using a parametrization of the measured π^0 p_T spectra [30] in a Monte Carlo decay generator, the p_T spectrum of daughter electrons is determined. The p_T spectra of the other light mesons that contribute to the cocktail (η, ρ, ω, η', and ϕ) are derived from the π^0 spectrum by m_T scaling (replacing p_T in the parametrization with $\sqrt{p_T^2 + m_{\rm meson}^2 - m_{\pi^0}^2}$) and then normalizing to the measured meson to pion ratios at high p_T. At intermediate p_T the contribution from J/ψ decays becomes significant and the measured p_T spectra [31] are fit and used as the parent p_T spectra in the decay generator. The cocktail of nonheavy flavor electrons is subtracted from the inclusive electron sample to isolate the contribution from open-heavy-flavor electrons. This method works well at larger p_T, where the heavy-flavor contribution is significant, but suffers from large systematic uncertainties at low electron p_T, where the ratio of open-heavy-flavor electrons to all electrons is low.

The second method of isolating the open-heavy-flavor yield uses a "converter" to deliberately increase the photonic background by a well-defined amount. In the standard PHENIX configuration, the number of inclusive electrons in a given p_T range $N_e^{\rm standard}$ can be expressed as

$$N_e^{\rm standard} = N^{\gamma} + N^{\text{non-}\gamma}, \tag{1}$$

where N^{γ} and $N^{\text{non-}\gamma}$ are the number of photonic and nonphotonic electrons in that p_T bin, respectively.

The converter is a sheet of brass, 0.25 mm thick, which has a radiation length determined to a precision of ±0.25%. For a portion of 2005 running, the converter was wrapped around the beam pipe. This extra material increases the real photonic electron background by an amount R_{γ} and reduces the nonphotonic electrons by a factor $(1-\epsilon)$, giving an inclusive electron yield in the converter configuration $N_e^{\rm converter}$ of

$$N_e^{\rm converter} = R_{\gamma} N^{\gamma} + (1-\epsilon) N^{\text{non-}\gamma}, \tag{2}$$

where the factors R_{γ} and ϵ are determined through simulation. R_{γ} has a slight p_T dependence that is prevalent in the low p_T region and plateaus at a value of 2.4, and $\epsilon = 0.021 \pm 0.005$. The uncertainties on these quantities are found by varying the

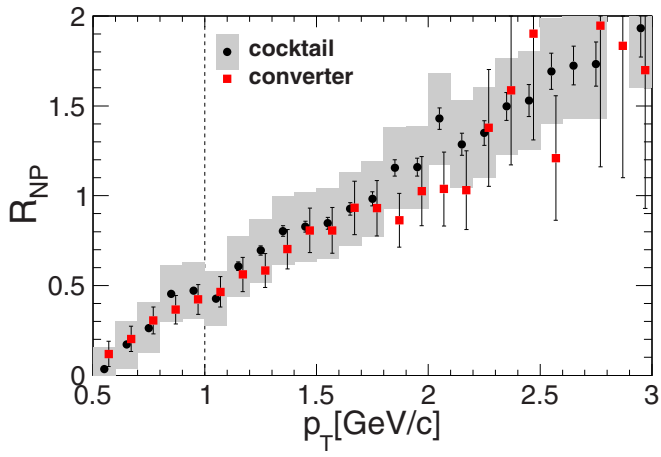

FIG. 2. (Color online) The ratio of nonphotonic to photonic electrons by the converter and cocktail methods, for MB Cu + Cu collisions. Gray bands are the systematic uncertainties on the cocktail method. For clarity, the converter points have been slightly displaced to the right.

radiation length of the converter material in simulation by the uncertainty in the measured converter thickness.

A simultaneous solution of Eqs. (1) and (2) gives the quantity of interest $N^{\text{non-}\gamma}$. The remaining nonphotonic background electrons are subtracted following the cocktail method previously described to isolate the open-heavy-flavor electron contribution. Because the converter produces an undesirable background for other measurements at PHENIX, it is only installed for a relatively short amount of time. Therefore, the converter method of background determination is limited by the statistics of the data sample taken with the converter installed. However, at low p_T, where statistical uncertainties are relatively small, the converter method provides meaningful results. Because this region is where the cocktail method is limited by systematic uncertainties, and high p_T is where the converter method is limited by statistics, the open-heavy-flavor electron results are determined by the converter method at $p_T < 1$ GeV/c, and by the cocktail method elsewhere. Additionally, there is no charged hadron data below 1 GeV/c to use for the cocktail and therefore the converter data is used there.

As a stringent cross check of the methods described here, the ratio of nonphotonic electrons to photonic electrons,

$$R_{\text{NP}} = \frac{N^{\text{non-}\gamma}}{N^{\gamma}}, \tag{3}$$

is compared for the two methods (shown in Fig. 2). The gray boxes are the systematic uncertainties in determining R_{NP} from the cocktail method.

Systematic uncertainties

The systematic uncertainties on the resulting heavy-flavor electron yield come from the determination of the inclusive electron yield and the uncertainty on the cocktail (converter) method. The uncertainties are explained in detail in Ref. [3] and are summarized here.

The systematic uncertainty on the inclusive yield is a combination of three parts: the uncertainty on the run group correction, eID, and geometric matching. For the ERT data set there is an additional uncertainty that comes from determining the trigger efficiency. The run-group-correction uncertainty comes from the fluctuation of the average number of electrons per event ($\langle N_e/N_{\text{evt}}\rangle$) for each run (where a run is defined as the data taken between successive starts of the PHENIX data acquisition system). The uncertainty on $\langle N_e/N_{\text{evt}}\rangle$ was found to be 1% and is assigned as the run-group-correction fluctuation. The uncertainty in identifying electrons comes from the inability to perfectly model the detector in simulation. It is estimated by repeating the acceptance × efficiency calculation for tighter and looser cuts, which are then applied to inclusive yields made with the same cuts. The ratio between the standard and tight or loose cuts is found to be 6% and is taken as the systematic uncertainty. Mismatching in the detector acceptance between simulation and data is an additional uncertainty and was found to be 4%. The ERT data set is only used in the high p_T region where the trigger efficiency is at the plateau value and so the only uncertainty is attributable to the determination of the trigger plateau, 2%. The total systematic uncertainty on the inclusive MB (ERT) yield is the quadrature sum of the previously discussed uncertainties and is found to be 7.3 (7.5)%.

The dominant systematic uncertainty on the cocktail comes from the uncertainty on the 2005 Cu + Cu neutral pion data [30] that is used as the input parent spectra for all of the light mesons. The pion data are moved up and down by their systematic uncertainties and refit. These new fits are then input into the decay generator and the output decay spectra become the upper and lower spread of the systematic uncertainties. The systematic uncertainty on the J/ψ spectra is done in the same manner as the pions. The rest of the light mesons are moved up and down by the uncertainty on the meson/π^0 ratios at high p_T. The systematic uncertainty on the conversion yield is found by scaling the conversion probability up and down by 10%. This gives a conservative estimate of the uncertainty on the amount of conversion material within PHENIX. The K_{e3} is assigned a 50% uncertainty as in previous analyses. The systematic uncertainty on the cocktail is dependent on p_T and centrality but has an average value of ∼12% for MB collisions.

The systematic uncertainty on the converter analysis comes from two sources: the already described uncertainty on the inclusive yield and the uncertainty derived from extracting a nonphotonic yield from the converter analysis. These uncertainties are independent and added in quadrature. R_γ,

TABLE II. Systematic uncertainties on the determination of the open-heavy-flavor yield of electrons for MB collisions.

Run group correction	1%
Acceptance × efficiency	6%
Geometric matching	4%
Trigger efficiency	2%
MB (ERT) inclusive yield	7.3% (7.5%)
Cocktail (Average)	12%
Converter	8%

ϵ, and $N_{\rm inc}^{C}$ are moved up and down by their systematic uncertainties and the effect on the yield is calculated and then added in quadrature. The overall converter systematic uncertainty is found to be 8% for MB. Table II summarizes the different systematic uncertainties.

IV. RESULTS FROM Cu + Cu COLLISIONS

The invariant yield of heavy-flavor electrons is calculated as a function of p_T using the following formula,

$$\frac{1}{2\pi p_T}\frac{d^2N^e}{dp_T dy} = \frac{1}{2\pi p_T N_{\rm events}}\frac{N_{e_{\rm HF}}}{2}\frac{1}{\Delta p_T \Delta y}\frac{1}{\epsilon_{\rm BBC}\epsilon_{\rm eID}}, \quad (4)$$

where $N_{\rm events}$ is the number of events, Δp_T is the p_T bin width, Δy is the rapidity range ($|y| < 0.35$), $\epsilon_{\rm BBC}$ is the BBC efficiency for MB (94%), $\epsilon_{\rm eID}$ is the acceptance and efficiency correction, and $N_{e_{\rm HF}}$ is the calculated number of heavy-flavor electrons and positrons from either the cocktail or converter method.

When plotting the invariant yield vs p_T, the average value is plotted at the bin center. However, for a steeply falling spectrum, the average value does not lie at the center of the bin. This is corrected by adjusting the average value over the bin to correspond to the value of the yield at the p_T bin center. This procedure assumes that the invariant yield as a function of p_T varies smoothly, which is a reasonable assumption. The p_T spectra of heavy-flavor electrons ($e_{\rm HF}$) produced in Cu + Cu collisions at $\sqrt{s_{NN}} = 200$ GeV are shown for five different centralities in Fig. 3, along with a fit to the $e_{\rm HF}$ spectrum from $p + p$ collisions (as reported in Ref. [3]) scaled by $\langle N_{\rm coll}\rangle$.

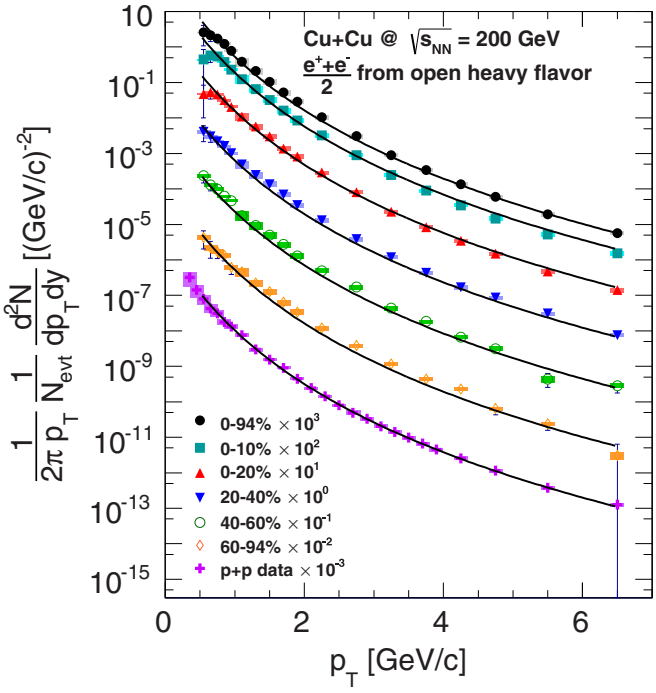

FIG. 3. (Color online) The p_T spectra of electrons from the decays of open-heavy-flavor hadrons produced in Cu + Cu collisions, separated by centrality. The lines are a fit to the $p + p$ data [3] scaled by $\langle N_{\rm coll}\rangle$.

To quantify nuclear effects, the nuclear modification factor R_{AA} is calculated according to

$$R_{AA} = \frac{dN^e_{A+A}/dp_T}{\langle N_{\rm coll}\rangle \times dN^e_{p+p}/dp_T}, \quad (5)$$

where dN^e_{A+A}/dp_T (dN^e_{p+p}/dp_T) is the differential yield in $A + A$ ($p + p$) collisions. An R_{AA} value of 1 indicates that the $A + A$ data are well described by a superposition of independent $p + p$ collisions. Following Refs. [3,18], at $p_T < 1.6$ GeV/c, R_{AA} is calculated by dividing the Cu + Cu spectra by the $p + p$ spectra point by point. The statistical (systematic) uncertainties on R_{AA} in this range are the quadrature sum of the statistical (systematic) uncertainties on the Cu + Cu and $p + p$ yields in a given p_T bin.

Above $p_T = 1.6$ GeV/c, where the $p + p$ data are well represented by the shape from fixed-order plus next-to-leading-log calculations from Ref. [32], a fit to that shape is used to represent the $p + p$ denominator. A function of the form

$$Y(p_T) = \frac{A}{(p_T + B)^n} \quad (6)$$

is fit to these data, where $A = 0.0067 \pm 0.0035$ (GeV/c)$^{-2}$, $B = 1.079 \pm 0.085$ GeV/c, and $n = 8.86 \pm 0.23$. Here the statistical uncertainty on R_{AA} is determined by the statistical uncertainty on the Cu + Cu spectra. The systematic uncertainty on R_{AA} is the quadrature sum of the systematic uncertainty on the $e_{\rm HF}$ yield from Cu + Cu and $p + p$ and the statistical uncertainty on the fit to the $p + p$ data. The global scaling uncertainty plotted around 1 is the quadrature sum of the global uncertainty on the $p + p$ spectra and the uncertainty on $\langle N_{\rm coll}\rangle$.

The centrality dependence of R_{AA} in Cu + Cu is shown in Figs. 4(a)–4(f). Figure 4(b) shows the nuclear modification factor for the 0%–10% most central Cu + Cu collisions, in which a moderate suppression of $e_{\rm HF}$ is observed for $p_T > 3$ GeV/c. This suppression is usually attributed to energy loss in the hot nuclear medium. Although this is a significant deviation from a superposition of independent $p + p$ collisions, the magnitude of suppression is smaller than what is seen in central Au + Au collisions [3,4].

In contrast, a significant enhancement is observed in more peripheral Cu + Cu collisions, Fig. 4. To quantitatively examine the difference within the Cu + Cu system itself, the $\langle N_{\rm coll}\rangle$-scaled ratio of the most central to most peripheral spectra $R_{\rm cp}$, defined as

$$R_{\rm cp} = \frac{N_{\rm coll}^{\rm peripheral}}{N_{\rm coll}^{\rm central}} \times \frac{dN^{\rm central}_{\rm Cu+Cu}/dp_T}{dN^{\rm peripheral}_{\rm Cu+Cu}/dp_T}, \quad (7)$$

is shown in Fig. 5. Most of the systematic uncertainties cancel in $R_{\rm cp}$, leaving only the uncertainty on the centrality dependent cocktail and the ratio of $\langle N_{\rm coll}\rangle$ values. A clear suppression is seen in the most central collisions relative to the most peripheral, which can be attributed to the suppression effects of the hot, dense partonic matter dominating in central collisions.

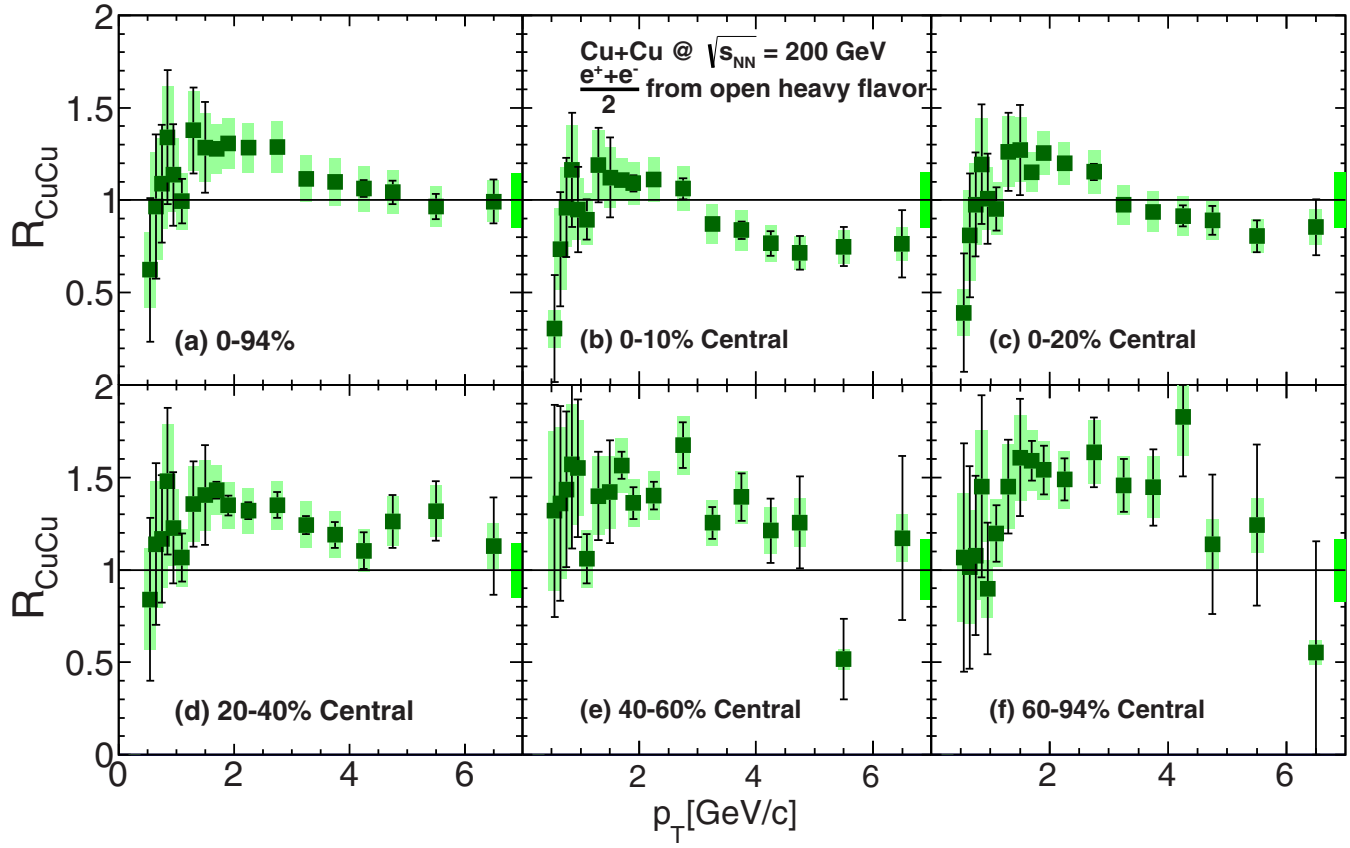

FIG. 4. (Color online) The nuclear modification factor for MB (0%–94%) and five centrality bins (0%–10%, 0%–20%, 20%–40%, 40%–60%, 60%–94%). The boxes around 1 are global uncertainties, which include the $\langle N_{\rm coll}\rangle$ scaling error and $p+p$ global uncertainty (9.9%) added in quadrature.

V. SYSTEM-SIZE DEPENDENCE

The full extent of the system-size dependence is directly illustrated by comparing the most central bins of all three systems in Fig. 6. There is a clear enhancement in central $d+$Au collisions, which gives way to a slight suppression in central Cu + Cu collisions, and finally a large suppression in the most central Au + Au bin.

If results from different systems are compared in centrality bins of comparable system size the trend is similar. Here we

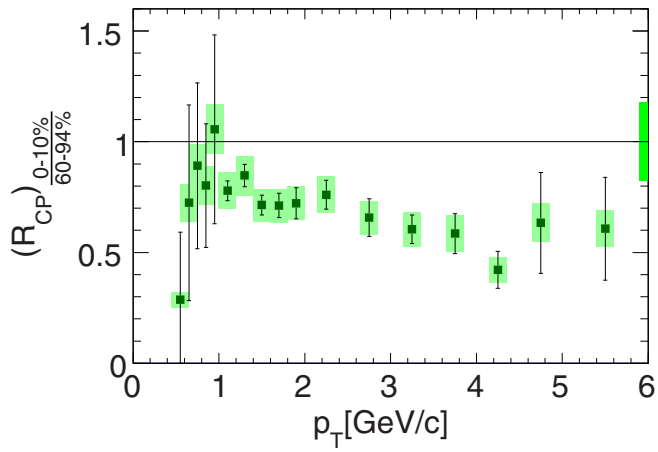

FIG. 5. (Color online) The ratio $R_{\rm cp}$ of the most central 0%–10% $e_{\rm HF}$ spectra to the most peripheral 60%–94%, scaled by $\langle N_{\rm coll}\rangle$. The global uncertainty on the determination of $\langle N_{\rm coll}\rangle$ for each centrality is shown as a box around 1.

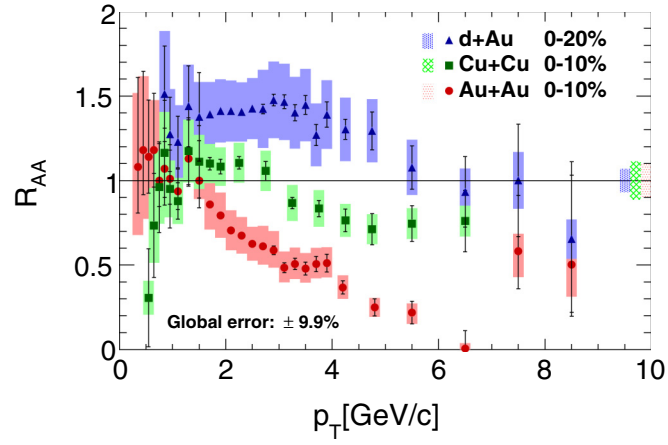

FIG. 6. (Color online) The nuclear modification factors for $e_{\rm HF}$ at midrapidity in central $d+$Au [18], Cu + Cu, and Au + Au [3] collisions at $\sqrt{s_{NN}} = 200$ GeV. The boxes around 1 are global uncertainties, which include the $\langle N_{\rm coll}\rangle$ scaling error. The global error given in the legend is from the $p+p$ yield.

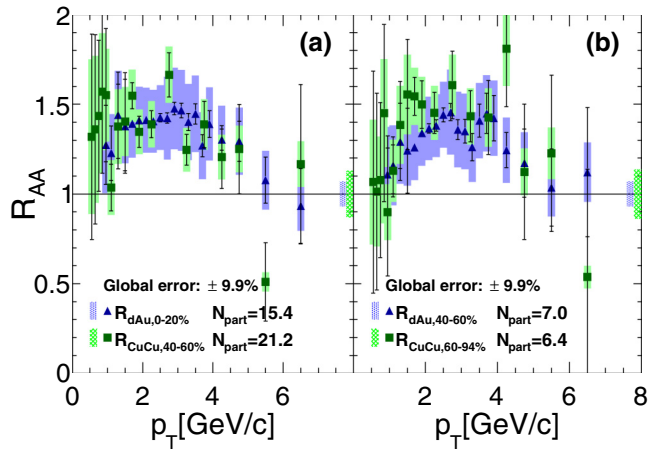

FIG. 7. (Color online) The nuclear modification factors for (a) 0%–20% d + Au [18] and 40%–60% Cu + Cu collisions and (b) 40%–60% d + Au and 60%–94% Cu + Cu collisions. The boxes around 1 are global uncertainties, which include the $\langle N_{\rm coll}\rangle$ scaling error. The global error given in the legend is from the $p + p$ yield.

take the number of nucleons participating in the collision, $\langle N_{\rm part}\rangle$, as a measure of the centrality and of the size of the system. Figure 7 shows overlays of the R_{AA} for peripheral Cu + Cu collisions with the R_{dA} for d + Au collisions at a comparable value of $\langle N_{\rm part}\rangle$. A similar enhancement is seen for the two systems.

Within the Cu + Cu system, the enhancement is overtaken by suppression as the average impact parameter decreases and with it the number of collisions increases. To compare the levels of suppression in Cu + Cu and Au + Au collisions, the nuclear modification factors for heavy-flavor electrons in centrality classes with comparable $\langle N_{\rm part}\rangle$ values are shown in Fig. 8. Here our centrality selections do not allow for as close a match, but a similar level of modification is seen for the different systems at similar values of $\langle N_{\rm part}\rangle$. We note that

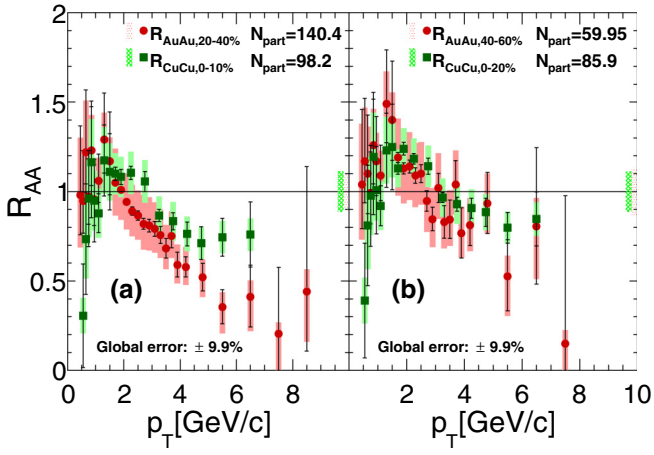

FIG. 8. (Color online) The nuclear modification factors for (a) 0%–10% Cu + Cu and 20%–40% Au + Au [3] collisions and (b) 0%–20% Cu + Cu and 40%–60% Au + Au collisions. The boxes around 1 are global uncertainties, which include the $\langle N_{\rm coll}\rangle$ scaling error. The global error given in the legend is from the $p + p$ yield.

if $\langle N_{\rm coll}\rangle$ were used instead as a measure of the system size the centrality bin selections would be the same (see Table I).

Rather than comparing R_{AA} vs p_T for similar system size, one can also compare average R_{AA} values in a given p_T range as a function of $\langle N_{\rm part}\rangle$ or $\langle N_{\rm coll}\rangle$. The average value of the nuclear modification factor for $1 < p_T < 3$ GeV/c and $3 < p_T < 5$ GeV/c for the three collision species is shown in Figs. 9 and 10, as a function of $\langle N_{\rm coll}\rangle$ and $\langle N_{\rm part}\rangle$, respectively. With the exception of the most peripheral Au + Au bin in the higher p_T range, a trend of increasing enhancement followed by suppression is seen among the three distinct systems, with Cu + Cu showing evidence of both. This common trend suggests that the enhancement and suppression effects are dependent on the size of both the colliding system and the produced medium.

VI. DISCUSSION

Charm and bottom production at midrapidity is dominated by gluon fusion and samples nuclear x values of $\sim 10^{-2}$, where modification of the gluon parton distribution function (PDF) may be significant in central collisions. Because the observed enhancement occurs in peripheral Cu + Cu collisions with a large average impact parameter, where the spatially dependent nuclear PDF is expected to have minimal changes from the free-nucleon PDF [33], this may suggest that gluon modification is not the dominant effect at midrapidity. Parton energy loss in the nucleus may also affect heavy-flavor production in nuclear collisions [17]. These effects are also expected to occur in the initial stages of central nuclear collisions, prior to the formation of the hot nuclear medium.

The heavy quark data from Cu + Cu collisions displays enhancement features at low p_T similar to those found in the d + Au collisions. This hardening of hadron spectra in nuclear collisions compared to $p + p$ collisions is known as the "Cronin effect" [34] and is used generically for $R_{AA} > 1$ observations. The Cronin effect is more structured than was expected, with both an observed mass dependence and a difference between baryons and mesons [35]. Early explanations of the mechanism behind the Cronin effect relied on k_T boosts to partons via scattering in the nucleus before the hard scattering and subsequent fragmentation [36]; however, this hypothesis does not explain the observed mass dependence, because the k_T transverse momentum kicks in the nucleus presumably occur before hadronization and therefore could not preferentially boost protons more than pions.

The enhancement seen for heavy-flavor electrons in central d + Au is larger than what is observed for pions and kaons at the same collision energy [37]. In central d + Au collisions, a mass-dependent enhancement is observed for identified pions, kaons, and protons [35]. The proton spectra show the largest enhancement and reach an R_{dA} of ~1.5 at $p_T = 3$ GeV/c in MB d + Au collisions. If Cronin enhancement is a purely mass-dependent effect, the D meson ($m \sim 1.1$ GeV) and proton ($m \sim 938$ GeV) should display a similar enhancement, while if the effect is driven by different dynamics of mesons and baryons, they should be different. Although the D-meson spectra have not been measured in d + Au collisions, the electrons show an enhancement that is comparable to protons.

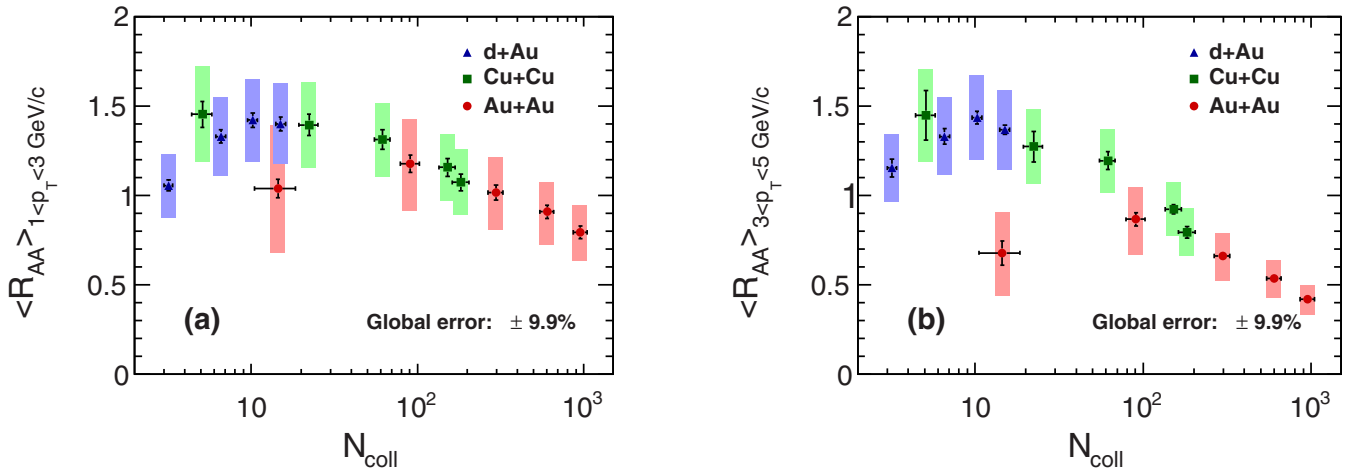

FIG. 9. (Color online) The nuclear modification factors, averaged over $1 < p_T < 3$ GeV/c (a) and $3 < p_T < 5$ GeV/c (b), for $e_{\rm HF}$ at midrapidity in d + Au [18], Cu + Cu, and Au + Au [3] collisions plotted as a function of $\langle N_{\rm coll}\rangle$.

However, the significant uncertainties on the electron spectrum preclude a precise comparison.

An alternative scenario involving recombination of soft partons in the hadronization process naturally gives a difference between meson and baryon enhancement [38,39], but it is not immediately clear what effect this has on heavy-flavor electrons, which are from a mixture of charm and bottom meson and baryon decays (though most are from mesons). The baryon enhancement observed in d + Au and $A + A$ collisions at RHIC can also suppress $e_{\rm HF}$ production at moderate p_T, because charmed baryons have a smaller branching ratio to electrons than charmed mesons [15]; however, currently no measurements of charmed baryons at RHIC energies exist to confirm any changes in the charmed hadron chemistry.

Several mechanisms were put forth to explain the large $e_{\rm HF}$ suppression in Au + Au collisions (shown in Fig. 8) when it was found that radiative energy loss alone was not sufficient to reproduce the suppression [40]. It was originally thought that heavy quarks would exhibit less suppression than light quarks in a deconfined medium, owing to a suppression of small-angle gluon radiation known as the "dead cone" effect [6]. However, the large suppression of $e_{\rm HF}$ on the same level as the π^0 in Au + Au contradicts that theory and/or suggests that there is something else contributing to the suppression of $e_{\rm HF}$.

It was found that over the p_T range measured at RHIC, radiative and collisional energy loss are comparable for heavy quarks [12]. In contrast to what was originally thought, collisional energy loss should be taken into account in energy-loss calculations. Recent models including collisional energy loss have been more successful at describing the Au + Au data [13,41].

Fragmentation and dissociation have recently been used to describe the suppression of the quarkonia yield in Au + Au collisions and could also be applied to the heavy-light bound states of the D and B mesons [42]. Previous models assume that the hard parton fragments in vacuum after fully traversing the medium and having lost energy through radiative and collisional processes. However, because of their large masses, B and D mesons can have formation times less than the length of the medium. The subsequent fragmentation and dissociation

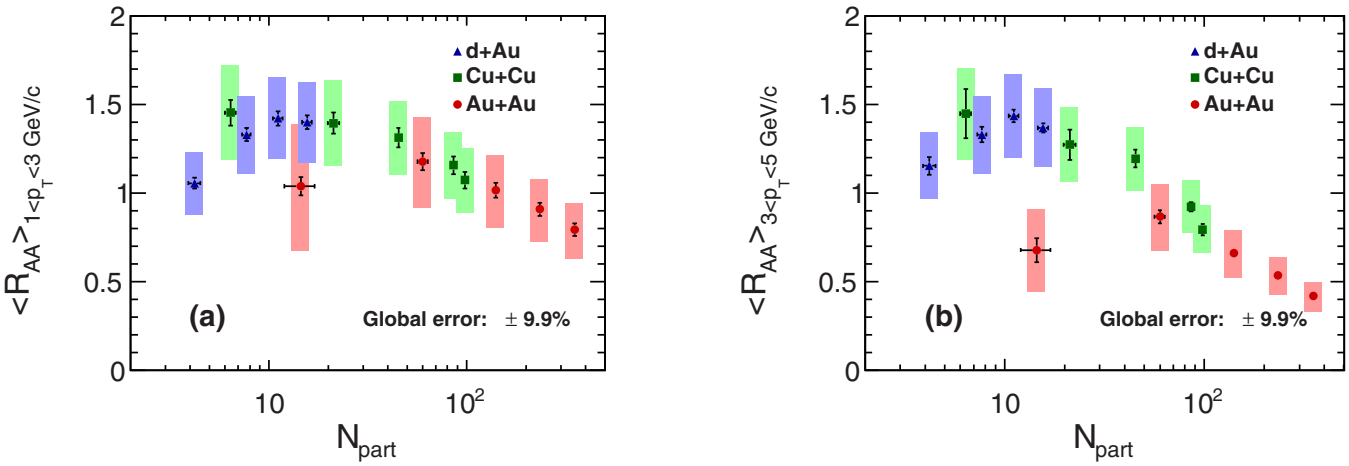

FIG. 10. (Color online) The nuclear modification factors, averaged over $1 < p_T < 3$ GeV/c (a) and $3 < p_T < 5$ GeV/c (b), for $e_{\rm HF}$ at midrapidity in d + Au [18], Cu + Cu, and Au + Au [3] collisions plotted as a function of $\langle N_{\rm part}\rangle$.

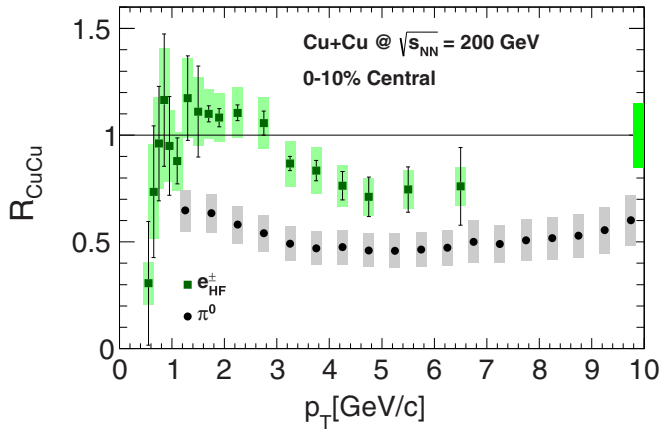

FIG. 11. (Color online) R_{AA} for π^0 and $e_{\rm HF}$. The boxes around 1 are global uncertainties, which include the $\langle N_{\rm coll}\rangle$ scaling uncertainty and $p+p$ global uncertainty.

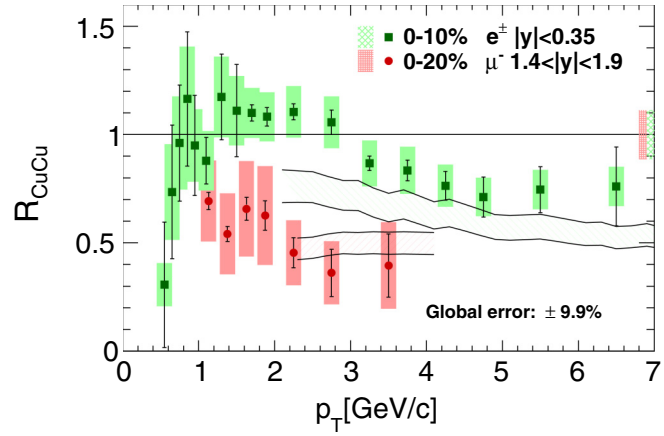

FIG. 12. (Color online) The nuclear modification factors for 0%–10% most central $e_{\rm HF}$ at midrapidity and 0%–20% most central $\mu^-_{\rm HF}$ at forward rapidity. The boxes around 1 are global uncertainties from the $\langle N_{\rm coll}\rangle$ scaling error. The global uncertainty is that on the $p+p$ yield. Model bands are calculations from [44], including partonic energy loss, energy loss from fragmentation and dissociation, and effects from nuclear matter.

of the heavy quarks and mesons can lead to a suppression in the heavy-flavor electron yield. This is particularly important for the B mesons because of their large masses. Calculations of in-medium dissociation [14,43] are in better agreement with the yield of $e_{\rm HF}$ in Au + Au collisions than those only including partonic energy loss. These effects are sensitive to the formation times of the mesons and the hot nuclear medium.

The $e_{\rm HF}$ and π^0 R_{AA} for central Cu + Cu collisions are shown in Fig. 11. Because the $e_{\rm HF}$ is the product of a charm or bottom hadron decay, its p_T is not that of the parent and thus direct comparisons to other hadronic spectra should take this into account. The π^0 are more suppressed than the $e_{\rm HF}$ over the limited p_T range of the electrons. While this may suggest a difference in energy loss for light and heavy quarks, the peripheral π^0 data show none of the enhancement that is present for heavy flavor. Because the nuclear effects are expected to be present in the initial state of central collisions, the different level of suppression for $e_{\rm HF}$ and π^0 may indicate that the initial-state effects on light and heavy quarks are different. A similar difference is also observed in d + Au collisions, where the $e_{\rm HF}$ show significant enhancement while the π^0 does not.

Previous PHENIX measurements at forward rapidity ($1.4 < y < 1.9$) showed a significant suppression of heavy-flavor muons ($\mu_{\rm HF}$) in central Cu + Cu collisions [45]. The magnitude of this suppression at forward rapidity in Cu + Cu (shown in Fig. 12) is comparable to the suppression of $e_{\rm HF}$ in central Au + Au collisions at midrapidity. This observation is difficult to reconcile with explanations of heavy-flavor suppression that depends solely on energy loss in the hot nuclear medium, because the energy density of the matter created in central Au + Au collisions is expected to be larger than in Cu + Cu collisions [45,46]. Because open heavy flavor is significantly more suppressed at forward rapidity than at midrapidity in Cu + Cu, additional nuclear effects, such as gluon shadowing at low x or partonic energy loss in the nucleus, may be significant. At RHIC, these low-x, shadowing effects are probed by looking in the forward direction, but at the Large Hadron Collider [47] these effects may also be relevant to heavy-flavor production at midrapidity, because the $\sqrt{s_{NN}}$ is higher than at RHIC and probes a lower x range within the nucleus.

The heavy-flavor electrons and muons are compared in Fig. 12 to a theoretical prediction that combines the effects of partonic energy loss and energy loss from fragmentation and dissociation and includes nuclear-matter effects such as shadowing and Cronin enhancement owing to parton scattering in the nucleus [44]. The model calculations were performed for 0%–10% most central collisions and are thus compared to the same centrality selection for the $e_{\rm HF}$. The most central bin of the $\mu^-_{\rm HF}$ from Ref. [45] is 0%–20% so that is plotted as a comparison. While consistent within uncertainties, the model predicts more suppression for heavy-flavor electrons than seen in the data. The B mesons are heavier and so dissociation is the dominant contribution to the energy loss for the entire p_T range at RHIC in this model. With its lighter mass, the D-meson transitions at $p_T \sim 5$ GeV/c to the traditional partonic energy loss. However, it is critical to test models against the full range of system sizes to have confidence in the underlying model physics and so calculations are needed for d + Au and peripheral Cu + Cu.

VII. SUMMARY AND CONCLUSIONS

The Cu + Cu data presented here build a bridge between the enhancement observed in d + Au collisions and the suppression found in Au + Au. We find that for electrons between 1 and 3 GeV/c the variation in R_{AA} is common as a function of $\langle N_{\rm part}\rangle$ or $\langle N_{\rm coll}\rangle$ in d + Au, Cu + Cu, and Au + Au. For electrons between 3 and 5 GeV/c this relation also holds with the exception of the most peripheral Au + Au collisions. Peripheral collisions of Cu nuclei display an enhancement of open heavy flavor at moderate p_T that is consistent with the enhancement observed in d + Au collisions at similar values of $\langle N_{\rm coll}\rangle$ and $\langle N_{\rm part}\rangle$, which suggests that significant effects on heavy quark production are present in

the initial state of heavy-ion collisions. In central Cu + Cu collisions, open heavy flavor at midrapidity is moderately suppressed when compared to a superposition of independent $p + p$ collisions and significantly suppressed compared to peripheral Cu + Cu collisions. The nuclear modification factor R_{AA} displays a suppression that is consistent with that seen in semiperipheral Au + Au collisions with a similar system size, suggesting that the suppressing effects from hot nuclear matter are becoming dominant.

While partonic energy loss in medium alone does not describe either the Cu + Cu or Au + Au $e_{\rm HF}$ data, a model which incorporates initial-state gluon shadowing, parton scattering and energy loss in nuclear matter, followed by dissociative energy loss in the hot medium, gives a reasonable description of central Cu + Cu open-heavy-flavor data at both midrapidity and forward rapidity. However, the mass dependence of different cold-nuclear-matter effects is still not reconciled. Further studies of these effects will only improve our understanding of the heavy-flavor electron data. Models that describe central Au + Au data should also be tested against the Cu + Cu and d + Au data. A number of different effects must be balanced to describe the data, which demonstrates the complicated interplay of effects from nuclear matter and those from the hot medium in heavy-ion collisions.

ACKNOWLEDGMENTS

We thank the staff of the Collider-Accelerator and Physics Departments at Brookhaven National Laboratory and the staff of the other PHENIX participating institutions for their vital contributions. We acknowledge support from the Office of Nuclear Physics in the Office of Science of the Department of Energy, the National Science Foundation, Abilene Christian University Research Council, Research Foundation of SUNY, and Dean of the College of Arts and Sciences, Vanderbilt University (U.S.A.); Ministry of Education, Culture, Sports, Science, and Technology and the Japan Society for the Promotion of Science (Japan); Conselho Nacional de Desenvolvimento Científico e Tecnológico and Fundação de Amparo à Pesquisa do Estado de São Paulo (Brazil); Natural Science Foundation of China (People's Republic of China); Ministry of Education, Youth and Sports (Czech Republic); Centre National de la Recherche Scientifique, Commissariat à l'Énergie Atomique, and Institut National de Physique Nucléaire et de Physique des Particules (France); Bundesministerium für Bildung und Forschung, Deutscher Akademischer Austausch Dienst, and Alexander von Humboldt Stiftung (Germany); Hungarian National Science Fund, OTKA (Hungary); Department of Atomic Energy (India); Israel Science Foundation (Israel); National Research Foundation and WCU program of the Ministry Education Science and Technology (Korea); Physics Department, Lahore University of Management Sciences (Pakistan); Ministry of Education and Science, Russian Academy of Sciences, Federal Agency of Atomic Energy (Russia); VR and Wallenberg Foundation (Sweden); the U.S. Civilian Research and Development Foundation for the Independent States of the Former Soviet Union; the US-Hungarian NSF-OTKA-MTA; and the US-Israel Binational Science Foundation.

[1] F. Karsch, Lect. Notes Phys. **583**, 209 (2002).
[2] A. Adare *et al.* (PHENIX Collaboration), Phys. Rev. Lett. **104**, 132301 (2010).
[3] A. Adare *et al.* (PHENIX Collaboration), Phys. Rev. C **84**, 044905 (2011).
[4] A. Adare *et al.* (PHENIX Collaboration), Phys. Rev. Lett. **98**, 172301 (2007).
[5] A. Adare *et al.* (PHENIX Collaboration), Phys. Rev. Lett. **97**, 252002 (2006).
[6] Y. L. Dokshitzer and D. Kharzeev, Phys. Lett. B **519**, 199 (2001).
[7] G. D. Moore and D. Teaney, Phys. Rev. C **71**, 064904 (2005).
[8] P. B. Gossiaux and J. Aichelin, Phys. Rev. C **78**, 014904 (2008).
[9] H. van Hees, V. Greco, and R. Rapp, Phys. Rev. C **73**, 034913 (2006).
[10] P. B. Gossiaux, R. Bierkandt, and J. Aichelin, Phys. Rev. C **79**, 044906 (2009).
[11] P. B. Gossiaux and J. Aichelin, J. Phys. G **36**, 064028 (2009).
[12] M. G. Mustafa, Phys. Rev. C **72**, 014905 (2005).
[13] S. Wicks, W. Horowitz, M. Djordjevic, and M. Gyulassy, Nucl. Phys. A **783**, 493 (2007).
[14] A. Adil and I. Vitev, Phys. Lett. B **649**, 139 (2007).
[15] P. Sorensen and X. Dong, Phys. Rev. C **74**, 024902 (2006).
[16] K. J. Eskola, H. Paukkunen, and C. A. Salgado, J. High Energy Phys. 04 (2009) 065.
[17] I. Vitev, Phys. Rev. C **75**, 064906 (2007).
[18] A. Adare *et al.* (PHENIX Collaboration), Phys. Rev. Lett. **109**, 242301 (2012).
[19] A. Adare *et al.* (PHENIX Collaboration), Phys. Rev. Lett. **111**, 212301 (2013).
[20] S. Chatrchyan *et al.*, Phys. Lett. B **718**, 795 (2013).
[21] B. Abelev *et al.* (ALICE Collaboration), Phys. Lett. B **719**, 29 (2013).
[22] G. Aad *et al.* (ATLAS Collaboration), Phys. Rev. Lett. **110**, 182302 (2013).
[23] K. Dusling and R. Venugopalan, Phys. Rev. Lett. **108**, 262001 (2012).
[24] L. McLerran, arXiv:0807.4095.
[25] K. Dusling and R. Venugopalan, Phys. Rev. D **87**, 054014 (2013).
[26] K. Dusling and R. Venugopalan, Phys. Rev. D **87**, 094034 (2013).
[27] K. Adcox *et al.* (PHENIX Collaboration), Nucl. Instrum. Methods A **499**, 469 (2003).
[28] M. L. Miller, K. Reygers, S. J. Sanders, and P. Steinberg, Annu. Rev. Nucl. Part. Sci. **57**, 205 (2007).
[29] R. Glauber and G. Matthiae, Nucl. Phys. B **21**, 135 (1970).
[30] A. Adare *et al.* (PHENIX Collaboration), Phys. Rev. Lett. **101**, 162301 (2008).
[31] A. Adare *et al.* (PHENIX Collaboration), Phys. Rev. Lett. **101**, 122301 (2008).
[32] M. Cacciari, P. Nason, and R. Vogt, Phys. Rev. Lett. **95**, 122001 (2005).
[33] I. Helenius, K. J. Eskola, H. Honkanen, and C. A. Salgado, arXiv:1205.5359.

[34] J. W. Cronin, H. J. Frisch, M. J. Shochet, J. P. Boymond, P. A. Piroué, and R. L. Sumner, Phys. Rev. D **11**, 3105 (1975).
[35] A. Adare *et al.* (PHENIX Collaboration), Phys. Rev. C **88**, 024906 (2013).
[36] A. Accardi, arXiv:hep-ph/0212148.
[37] S. S. Adler *et al.* (PHENIX Collaboration), Phys. Rev. Lett. **98**, 172302 (2007).
[38] R. C. Hwa and C. B. Yang, Phys. Rev. C **70**, 024905 (2004).
[39] R. C. Hwa and C. B. Yang, Phys. Rev. Lett. **93**, 082302 (2004).
[40] S. Wicks, W. Horowitz, M. Djordjevic, and M. Gyulassy, Nucl. Phys. A **784**, 426 (2007).
[41] B. W. Zhang, E. Wang, and X. N. Wang, Phys. Rev. Lett. **93**, 072301 (2004).
[42] C.-Y. Wong, Phys. Rev. C **72**, 034906 (2005).
[43] F. Dominguez and B. Wu, Nucl. Phys. A **818**, 246 (2009).
[44] R. Sharma, I. Vitev, and B.-W. Zhang, Phys. Rev. C **80**, 054902 (2009).
[45] A. Adare *et al.* (PHENIX Collaboration), Phys. Rev. C **86**, 024909 (2012).
[46] J. D. Bjorken, Phys. Rev. D **27**, 140 (1983).
[47] B. Abelev *et al.* (ALICE Collaboration), Phys. Rev. D **86**, 112007 (2012).